scientific reports

Check for updates

OPEN

Putative long range mossy fiber sprouting and regional cytochrome c oxidase alteration in the hippocampus of patients with mesial temporal lobe epilepsy

Tian Tu[1,2]✉, Lily Wan[2], Qi-Lei Zhang[2], Chen Yang[2], Hong-Shu Zhou[3], Zhong-Ping Sun[2], Hong-Yu Long[1], Bei-Sha Tang[1], Aihua Pan[2], Ewen Tu[4], Jian Wang[5], Zhi-Quan Yang[3], Zhen-Yan Li[3]✉ & Xiao-Xin Yan[2]✉

Mesial temporal lobe epilepsy (MTLE) is known as a distributed network disorder, and regional neuroanatomical changes may significantly contribute to aberrant network formation. The major pathologies of MTLE include neuronal loss in the dentate hilus, CA3 and CA1 regions, and mossy fiber (MF) sprouting into the inner molecular layer (iML). The latter forms aberrant excitatory circuities that are considered to facilitate recurrent seizures. The subiculum is relatively preserved during hippocampal sclerosis but has been thought to play a critical role in the synchronization and propagation of epileptic activity especially to extrahippocampal brain regions. We recently identified a distinct expression of alpha-smooth muscle actin (αSMA) at the MF terminals in human hippocampus. This prompted us to explore MF sprouting in resected hippocampi ($n = 20$) from patients with MTLE relative to postmortem control ($n = 20$) using αSMA along with reference markers for pathological cross-validation. Immunolabeling of neuron-specific nuclear antigen and sortilin showed neuronal loss in the hilus/CA3 and CA1 and granule cell dispersion in all resected hippocampi relative to control. Immunolabeling of αSMA, zinc transporter 3 and β-secretase 1 displayed a widening of the iML with enhanced staining intensity and a fibrous band extending from CA2, CA1 towards subiculum in the resected hippocampi. Cytochrome c oxidase immunolabeling was increased in the iML and subiculum in the MTLE group. Taking together, the current findings suggest the possibility of long-range MF sprouting and regionally occurred hypermetabolic state in the hippocampal formation of patients with drug resistant MTLE.

Keywords Aberrant neuroplasticity, Actin isoforms, Epilepsy, Hippocampal sclerosis, Neuronal death, Tri-synaptic circuit

Mesial temporal lobe epilepsy (MTLE) is a devastating neurological disease, especially affecting children and young adults who are expected to fulfill immense life and career potentials[1]. MTLE can be progressive, with hippocampal sclerosis and relapsing seizures worsening to a certain point with symptoms becoming pharmacologically uncontrollable[2]. Neuronal loss, gliosis, granule cell dispersion and mossy fiber (MF) sprouting are the pathological characteristics of MTLE[3]. According to the pathological grading system of the International League Against Epilepsy (ILAE)[4], neuronal loss and gliosis occur earlier and severely in the hilar region of the dentate gyrus (DG), CA3 and CA1, but can extend into CA2 and even the subicular subregions as sclerosis progresses. Granule cell dispersion involves increased cellular tiers and dislocation, reduced cell

[1]Department of Neurology, Xiangya Hospital, Central South University, Changsha 410008, Hunan, China. [2]Department of Anatomy and Neurobiology, Central South University, Xiangya Basic Medical School, Changsha 410013, Hunan, China. [3]Department of Neurosurgery, Xiangya Hospital, Central South University, Changsha 410008, Hunan, China. [4]Department of Neurology, The Second People's Hospital of Hunan Province, Changsha 410007, Hunan, China. [5]The Reproductive and Stem Cell Engineering Institute, Central South University Xiangya Basic Medical School, Changsha 410013, Hunan, China. ✉email: tutian1991@163.com; lizhenyan@csu.edu.cn; yanxiaoxin@csu.edu.cn

density and laminar disorganization. MF sprouting into the inner molecular layer (iML) has been commonly assessed using the histological Timm staining that detects the deposition of metal ions especially zinc in axonal terminals[5,6]. Other studies evaluate MF pathology (spouting into the iML and loss in the hilus) in animal brains and/or resected human hippocampal samples by immunohistochemical labeling of various presynaptic markers, including zinc transporter 3 (ZnT3)[7,8], dynorphin[9], vesicular glutamate transporters[10], synaptic vesicle proteins[6–8,11,12], and β-secretase 1 (BACE1)[11,12].

The sprouting MF terminals can form aberrant asymmetric synapses with the dentate granule cells, surviving hilar mossy cells and interneurons[10,13–16]. The reorganized MF terminals in the iML can develop the so-called perforated synapses, which are considered highly efficacious in synaptic transmission[9,17]. MF sprouting has been suggested to facilitate recurrent epileptiform activity in the DG[18,19], while this has remained an issue of debate as blocking MF sprouting by rapamycin does not reduce seizure frequency in pilocarpine-treated mice[20] and there also exists increased MF innervation to interneurons in the DG[21,22]. Studies in rodent models show that both neonatal and adult-born granule cells contribute to the formation of aberrant MF connections[23–26] and that optogenetic activation of sprouted MFs can detonate aberrant dentate network activity[27].

The subiculum is relatively preserved during hippocampal sclerosis and has been proposed to play a key role in the synchronization and propagation of neuronal hyperactivity into extrahippocampal brain regions[28]. Animal model and ex vivo human hippocampus studies have gained much electrophysiological and neuroanatomical evidence supporting this notion. The underlying mechanism includes enhanced excitatory and reduced inhibitory neuronal activity and altered glial modulation in this region[29–36]. The subiculum is therefore considered an area for potential pharmacological and surgical (such as deep brain stimulation) intervention for MTLE[37].

We recently identified a novel alpha-smooth muscle actin (αSMA) expression in human hippocampal MF[38]. Specifically, αSMA immunolabeling distinctly visualized the hippocampal MF terminals in postmortem postnatal and adult human brains in addition to blood vessels, while it only occurred at vasculature in other anatomical regions. Thus, we set to explore MF pathology in resected hippocampi from patients with MTLE with postmortem human brain samples as control using αSMA and established markers for MF sprouting and neuronal loss[38,39]. To understand a metabolic basis for hippocampal hyperexcitability, we assessed the expression of cytochrome c oxidase (COX) in the resected and control sections by immunohistochemistry.

Materials and methods

Resected hippocampi and postmortem control samples

Human brain materials were used in the current study with the approval (2020KT-37, 4/10/2020; #2023-KT084, 6/21/2023) by the Ethics Committee of Central South University Xiangya School of Medicine in compliance with the Code of Ethics of the World Medical Association (Declaration of Helsinki). All experimental procedures and methods were performed in accordance with the relevant guidelines and regulations set forth by Central South University. A total of 20 resected hippocampi were obtained from the Department of Neurosurgery of Xiangya Hospital following operation on patients with drug-resistant epilepsy and neuroimaging diagnosis of hippocampal sclerosis (Table 1). The samples were obtained between December 2020 and July 2022, with all patients remaining seizure-free to date. The surgical procedure and pathological examination of resected brain tissues were carried out with written consent from the patients and family members. The resected brain samples consisted of mostly the sclerotic hippocampus except for a few cases with fractional temporal cortical tissue. The samples available for this study were mostly a coronal slice at the mid-hippocampal level approximately in 0.5 cm thickness. The samples were placed on ice following resection, brought to a nearby pathological laboratory and dissected for use for this and other (ongoing) studies within approximately 30 min. The tissue slices used for the present study were fixed by immersion in formalin for 1–2 weeks.

Postmortem human brains were banked through a willed body donation program[40]. Each brain was bisected after removal from the skull, with a half cut into 1 cm-thick coronal slices, fresh-frozen then stored at -80 °C, and the other hemibrain immersed in formalin for 2–4 weeks and subsequently cut coronally into 1 cm-thick slices. Fixed brain blocks were prepared into cryostat (35 μm-thick) and paraffin (3 μm-thick) sections, followed by neuropathological evaluation for the presence of Alzheimer's and Parkinson disease pathologies according to the Standard Brain Banking Protocol proposed by China Brain Bank Consortium[41]. The postmortem brains were selected as control for the resected hippocampal group in an age/sex matchable manner, all of which lacked the above and other neuropathological lesions (Table 1).

Tissue preparation, histological and immunohistochemical stainings

In general, the surgically removed hippocampi from patients and temporal lobe slices from postmortem human brains were cryoprotected following formalin fixation in 30% sucrose until tissue sank, embedded in optimal cutting temperature (OCT) compound, cut in a cryostat into 35 μm-thick sections, which were stored in a cryoprotectant (30% sucrose, 30% ethylene glycol and 1% polyvinylpyrrolidone-40 (PVP-40 in 0.1 M phosphate buffer, pH 7.3) at -40 °C until use.

Cryostat sections were immunohistochemically stained in a batch-processing manner in 6-well tissue culture plate by including sections from 3 to 5 resected hippocampi and 3–5 postmortem brains in each experiment using the avidin-biotin complex (ABC) method (see Table 2 for antibody information). Selected sections were treated first in 0.1 M phosphate-buffer saline (PBS, pH 7.3) with 5% normal horse serum, 5% H_2O_2 and 0.1% Triton-100 for 1 h (hr) at room temperature to block nonspecific reactivity, then reacted with a primary antibody at 4 °C overnight. On the second day, the sections were incubated in PBS containing biotinylated pan-specific secondary antibody for 1 h and further reacted with the ABC reagent (1:200) for another hr at room temperature. Immunoreaction product was developed in PBS containing 0.05% diaminobenzidine (DAB) and 0.3% H_2O_2. A few sections were included in each experiment throughout all steps but the primary antibody incubation, which

Group	Case #	Age (year)	Sex	Clinical diagnosis or death cause	Post surgery or postmortem delay (hour)
Resected age=33.4±16.9 year; M/F=15/5	1	37	F	Drug-resistant MTLE, left hippocampal sclerosis	0.5
	2	27	F	Drug-resistant MTLE, left hippocampal sclerosis	0.5
	3	13	M	Drug-resistant MTLE, left hippocampal sclerosis	0.5
	4	45	M	Drug-resistant MTLE, left hippocampal sclerosis	0.5
	5	33	M	Drug-resistant MTLE, left hippocampal sclerosis	0.5
	6	52	F	Drug-resistant MTLE, left hippocampal sclerosis	0.5
	7	43	M	Drug-resistant MTLE, left hippocampal sclerosis	0.5
	8	36	M	Drug-resistant MTLE, right hippocampal sclerosis	0.5
	9	25	M	Drug-resistant MTLE, right hippocampal sclerosis	0.5
	10	24	M	Drug-resistant MTLE, left hippocampal sclerosis	0.5
	11	23	F	Drug-resistant epilepsy, complex partial seizure	0.5
	12	53	M	Focal epilepsy, right hippocampal sclerosis	0.5
	13	31	F	Drug-resistant epilepsy, complex partial seizure	0.5
	14	15	M	Drug-resistant epilepsy, complex partial seizure	0.5
	15	18	M	Drug-resistant MTLE, left hippocampal sclerosis	0.5
	16	19	M	Drug-resistant MTLE, right hippocampal sclerosis	0.5
	17	8	M	Drug-resistant MTLE, left hippocampal sclerosis	0.5
	18	32	M	Drug-resistant MTLE, right hippocampal sclerosis	0.5
	19	73	M	Epilepsy, multiple right temporal lobe access	0.5
	20	60	M	Epilepsy, right temporal lobe astrocytoma	0.5
Control age=36.0±17.9year; MF/=13/7	1	8	M	Leukemia	3
	2	14	M	Leukemia	9
	3	16	F	Leukemia	6
	4	18	M	Gliaoma	9
	5	21	M	Leukemia	5
	6	22	F	Systemic lupus erythematosus	12
	7	24	M	Leukemia	8
	8	28	M	Lung cancer	2
	9	29	F	Gastric carcinoma	6
	10	31	F	Leukemia	11
	11	33	F	Colon cancer	6
	12	38	M	Liver cancer	8
	13	46	F	Ovarian cancer	12
	14	47	M	Lung cancer	7
	15	49	M	Lung cancer	10
	16	51	M	Lymphoma	9
	17	54	M	Intracranial hemorrhagic stroke	6
	18	55	M	Asthma attack	9
	19	65	M	Esophageal cancer	3
	20	70	F	Diabetic heart failure	7

Table 1. Demographic information of the resected hippocampi and postmortem control samples.

Reagent	Source	Identifier
Rabbit polyclonal anti-αSMA	Sigma-Aldrich	Cat# ABT1487;RRID: AB_3094617
Rabbit monoclonal anti-BACE1	Abcam	Cat# ab183612; RRID: AB_3094757
Goat polyclonal anti-Sortilin	R&D Systems	Cat# AF3154; RRID: AB_2286389
Mouse monoclonal anti-NeuN	Sigma-Aldrich	Cat# MAB377; RRID: AB_2298772
Rabbit polyclonal anti-ZnT3	Proteintech	Cat# 17363-1-AP; RRID: AB_2239335
Mouse monoclonal anti-NPY	Santa Cruz Biotechnology	Cat# sc-133,080; RRID: AB_2298657
Biotinylated horse anti-mouse/rabbit/goat IgG antibody (H+L)	Vector Laboratories	Cat# BA-1300; RRID: AB_2336188
Vectastain Elite ABC kit	Vector Laboratories	Cat# PK-6100

Table 2. Key Immunolabeling resources used in the present study.

were used for defining background labeling. All the stained sections were mounted on glass microslides, allowed to air-dry, and coverslippered with a permanent mounting medium following dehydration and clearance in xylene.

Image acquisition and densitometric analyses

The sections were scan-imaged with the 20× objective on a Motic-Olympus microscope using the same imaging setting. Images were examined on the interface of the Motic Digital Slide Assistant System Lite 2.0 (Motic Asia, Hong Kong, China), with the areas of interest at desired magnifications extracted for quantification and figure preparation. To avoid confusion with different uses of the term "CA4", the area occupied by the pyramidal cells within the arc of the DG was considered a part of CA3 in the current study[42,43].

For neuron-specific nuclear antigen (NeuN) and sortilin immunolabeling, cell count was performed on the interface of the Motic imaging analysis system using a randomized sampling approach with the application of grids over the section image[44]. Counting zones consisted of 200 µm × 200 µm grids over the subregions of the hippocampal formation were randomly generalized in reference to the scales on the X and Y axes. We used 10–30 randomly generalized counting zones to estimate cell density in the hilus/CA3, CA1 and subicular areas in a given hippocampal section according to its size, with 5–10 zones used for counting in the CA2 area. Labeled somata were counted in each grid by experimenters who were blinded to the sample groups, with the mean densities (number of cells/µm2) in a given anatomical region calculated based on data obtained from two sections from each case.

Optic densitometry was carried out to measure αSMA, BACE1, ZnT3 and COX immunolabeling over subregions or lamina of the hippocampal structures using the OptiQuant software[11,45]. The original images from the MTLE and control groups were assembled together and saved as a TIFF file in grey-scale format. Total optic density (o.d.,), expressed as digital light units per square millimeter (DLU/mm2), was measured over the area of interest using the free-hand drawing tool. Thus, the total o.d. over the inner and outer molecular layers (iML and oML), the hilus and CA3 areas together, CA2, CA1, the subicular subregions together and a white matter area between the hippocampus and temporal cortex were obtained in the same immunostained section. The specific o.d. over the hippocampal regions in each sample were calculated using the density of the white matter area as a threshold cutoff.

Data processing, statistical analysis and figure Preparation

Densitometric data were processed in Excel spreadsheets, including grouping, normalization and calculation of means and standard deviation. Considering the resected hippocampi were fixed following surgical removal while the control samples were fixed with postmortem delays, we normalized the optic density data to the overall means (calculated by including values from all areas from all samples) of the two sample groups, respectively, for each type of immunolabeling. The normalized data were imported into GraphPad spreadsheets (GraphPad Prism 10) and analyzed statistically using one-way analysis of variance (ANOVA) with Tukey's multiple comparison *posthoc* tests, with $P < 0.05$ set as the cutoff for significant difference. Figures were prepared with Photoshop 2024 by assembling representative micrographs and graphs from data analyses. The overall brightness/contrast of figure panels was adjusted for proper visibility.

Results

Neuronal loss and granule cell dispersion in the resected hippocampi relative to control

Neuronal loss and granule cell dispersion are the key neuropathological features of MTLE; therefore we first assessed the pattern and extent of these changes in the resected hippocampi using NeuN immunolabeling for all neurons[4] (Fig. 1), and sortilin immunolabeling for principal neurons[45,46](Fig. 2). Neuronal loss was found to have reached CA1 in all resected hippocampi with variability between samples and could be seen in the subicular subregions in severely sclerotized hippocampi (Figs. 1A-F and 2A-F). Labeled neuronal profiles were also reduced apparently in the hilus and CA3 area within the arc of the DG among most cases, and, to a lesser extent, in the CA3 segment outside DG. Neuronal profiles were better preserved in CA2 and the joining CA3 and CA1 areas in a given hippocampus (Figs. 1A-E and 2A-E). However, the remaining pyramidal neurons in this sector appeared to be misaligned, had increased intercellular space and shortened apical dendritic processes by closer examination, relative to their counterparts in control sections (Fig. 2D1, F1). Granule cell dispersion was evident in the resected hippocampi, with the granule cells dislocated to the ML and formed bizarre-looking islands (Fig. 1B, B2; 2A). It should be noted that the NeuN-labeled neurons remained in CA1 were variable in size and appeared to be largely interneurons (Fig. 1C, C1). In comparison, the remaining sortilin-labeled neurons in this area had a relatively large soma with basal and apical dendritic processes, therefore appeared to represent the individually surviving pyramidal neurons (Fig. 2C, C1).

Cell count was originally performed over the hilus, CA3, CA2, CA1, and the subicular subregions (Sub) together. However, the CA3 areas within and outside the hilar region were difficult to define in the resected hippocampi due to the cell loss. Also considering that neuronal loss was generally parallel in the hilar and CA3 areas among the resected samples, we combined the densities obtained from these subareas together in both MTLE and control groups at the final data assembly (Figs. 1F and 2G). The densities (mean ± S.D.) of NeuN labeled profiles in the hilus/CA3 region were 44.5 ± 27.6 cells/mm^2 in the MTLE and 196.7 ± 68.1 cells/mm^2 in the control groups, respectively. The densities of NeuN labeled profiles were 297.7 ± 165.1 vs. 502.9 ± 141.7 cells/mm^2 in CA2, 149.4 ± 64.7 vs. 365.3 ± 178.1 cells/mm^2 in CA1 and 274.6 ± 67.8 vs. 322.2 ± 116.9 cells/mm^2 in Sub in the MTLE vs. control groups, respectively. There was an overall statistically significant difference of the means among the sample and region groups by one-way ANOVA [$P < 0.0001$; F (DFn, DFd) = 29.3 (7, 151)]. Significant differences were reached between the two sample groups for the means in hilus/CA3, CA2, CA1, but not Sub, by *posthoc* Tukey's multiple comparisons test (Fig. 1F). The extents of neuronal loss measured with sortilin

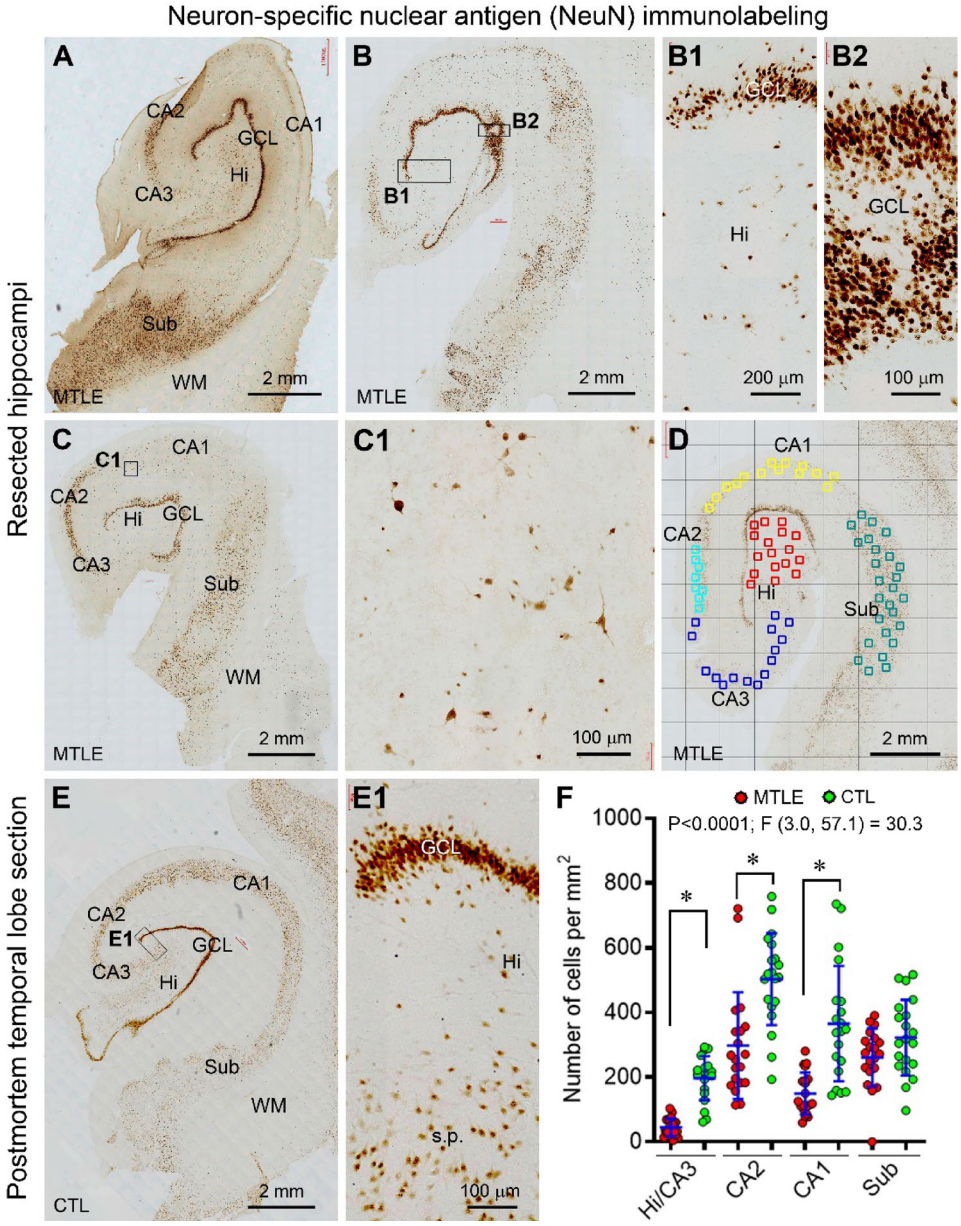

Fig. 1. Assessment of neuronal loss in resected hippocampi from patients with mesial temporal lobe epilepsy (MTLE) relative to control with neuron-specific nuclear antigen (NeuN) immunohistochemistry. Shown are microscopical images from four resected hippocampi and a postmortem control (CTL), with enlarged views as indicated. The labeled cellular profiles are greatly lost in CA1 in the resected samples (**A**, **B**, **B1**, **C**, **C1**, **D**) compared to CTL (**E**, **E1**), with neuronal loss also seen in the former in CA3, subiculum (Sub) (**B**, **C**) and CA2 (**D**) with variations between samples. Pyramidal neurons in CA2 and the joining CA3 and CA1 areas are relatively preserved in the resected sections (**A**, **C**). Granule cell dispersion is present in the resected hippocampi (**A**, **B**, **B2**, **C**), with ectopic granule cells forming bizarre-looking islands (**B2**). Panel (**D**) shows the cell counting method used in this study, with the numerical densities of labeled neurons from the hilus (Hi) and CA3 combined at final data assembling. Report of ANOVA test for the numerical cell densities of the regions and groups is placed in the graph, with the asterisk symbol (*) indicating statistically significant intergroup differences according to Tukey's multiple comparisons *posthoc* test (**F**, same format for other figures). Additional abbreviations: GCL: granule cell layer; s.p.: stratum pyramidale; WM: white matter. Scale bars are as indicated.

immunolabeling in principal neurons showed a similar trend as with that of NeuN labeling. Thus, the numerical densities of sortilin-labeled neurons were 51.2 ± 31.2 vs. 219.7 ± 51.0 cells/mm^2 in hilus/CA3, 299.4 ± 166.2 vs. 547.1 ± 108.8 cells/mm^2 in CA2, 116.9 ± 93.3 vs. 379.3 ± 54.5 cells/mm^2 in CA1 and 227.4 ± 74.2 vs. 312.8 ± 64.1 cells/mm^2 in Sub in the MTLE and control groups, respectively. There was also an overall difference in the

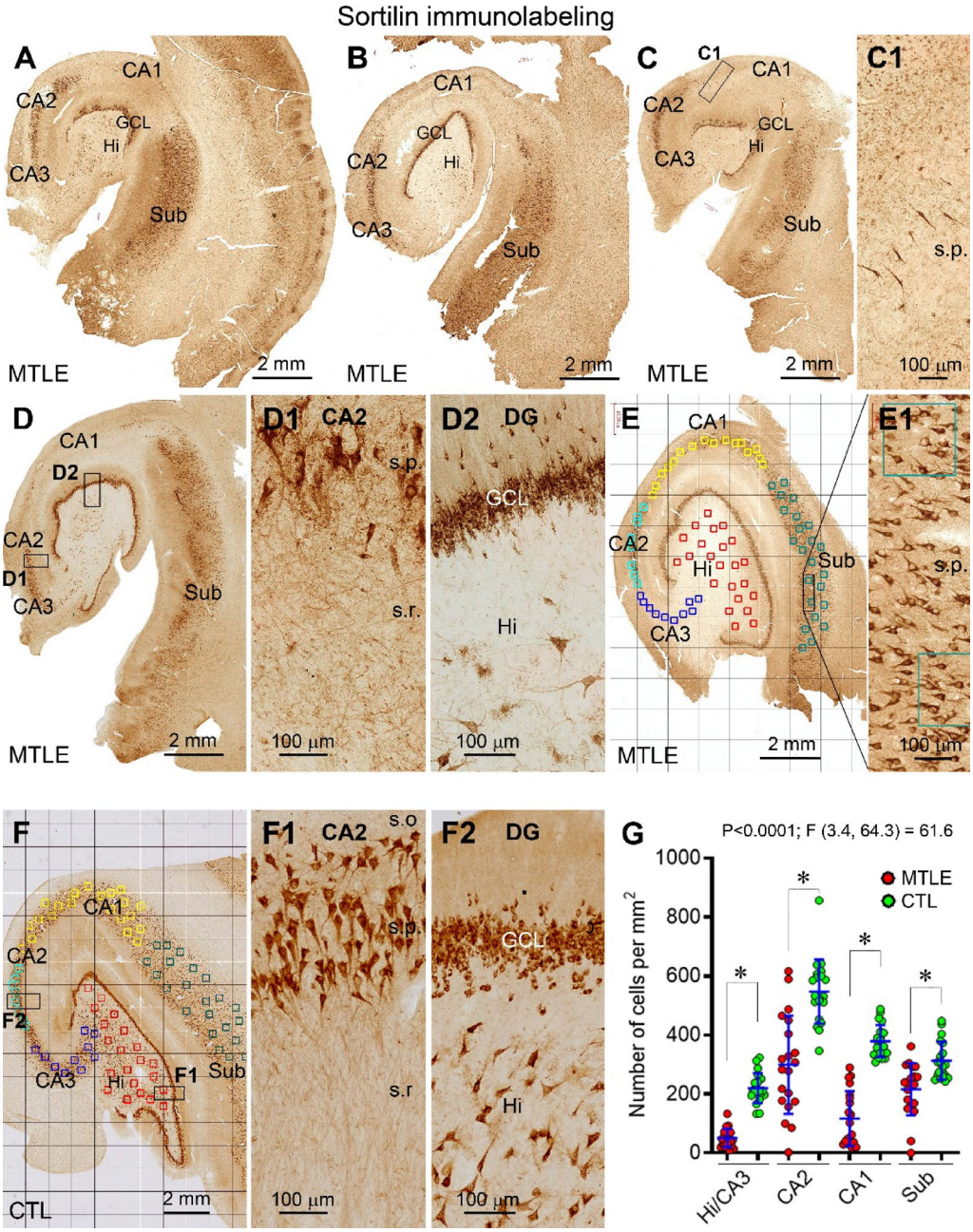

Fig. 2. Assessment of neuronal loss in resected hippocampi relative to control with sortilin immunohistochemistry. Shown are microscopical images from five resected hippocampi from patients with mesial temporal lobe epilepsy (MTLE) (**A**-**E**) and a postmortem brain as control (CTL) (**F**). Loss of the labeled neurons is seen in the hilus (Hi), CA3 and CA1 (**A**, **B**, **C**, **D**) and also in the subiculum (Sub) with variability between samples (**B**, **C**). Panel (**C1**) shows a few remaining pyramidal neurons in the striatum pyramidale (s.p.) of CA1. The pyramidal neurons in CA2 in the resected hippocampus are misaligned and separated from each other, and had fewer and shortened dendrites, in comparison with their counterpart in the control section (**D1**, **F1**). Dislocation of granule cells and loss of hilar mossy cells are clearly seen in the sclerotic (**D2**) as compared to the control (**F2**) hippocampus. Panels (**E**, **E1**) show cell counting in grided zones in the hippocampal subregions. Additional abbreviations: GCL: granule cell layer; s.o.: stratum oriens; s.r.: stratum radiatum. Scale bars are as indicated.

means [$P < 0.0001$; F (DFn, DFd) = 59.2 (7, 151)], with Tukey's posthoc tests indicating statistically significant differences of the means in the hilus/CA3, CA2, CA1 and Sub regions between the two samples groups (Fig. 2G).

Aberrant αSMA Immunolabeling in the resected hippocampi relative to control

The neuropil-type, but not the vascular, αSMA immunoreactivity (IR) was altered in the resected hippocampi relative to postmortem controls (Fig. 3). We referred "αSMA IR" to this neuronal labeling exclusively in the

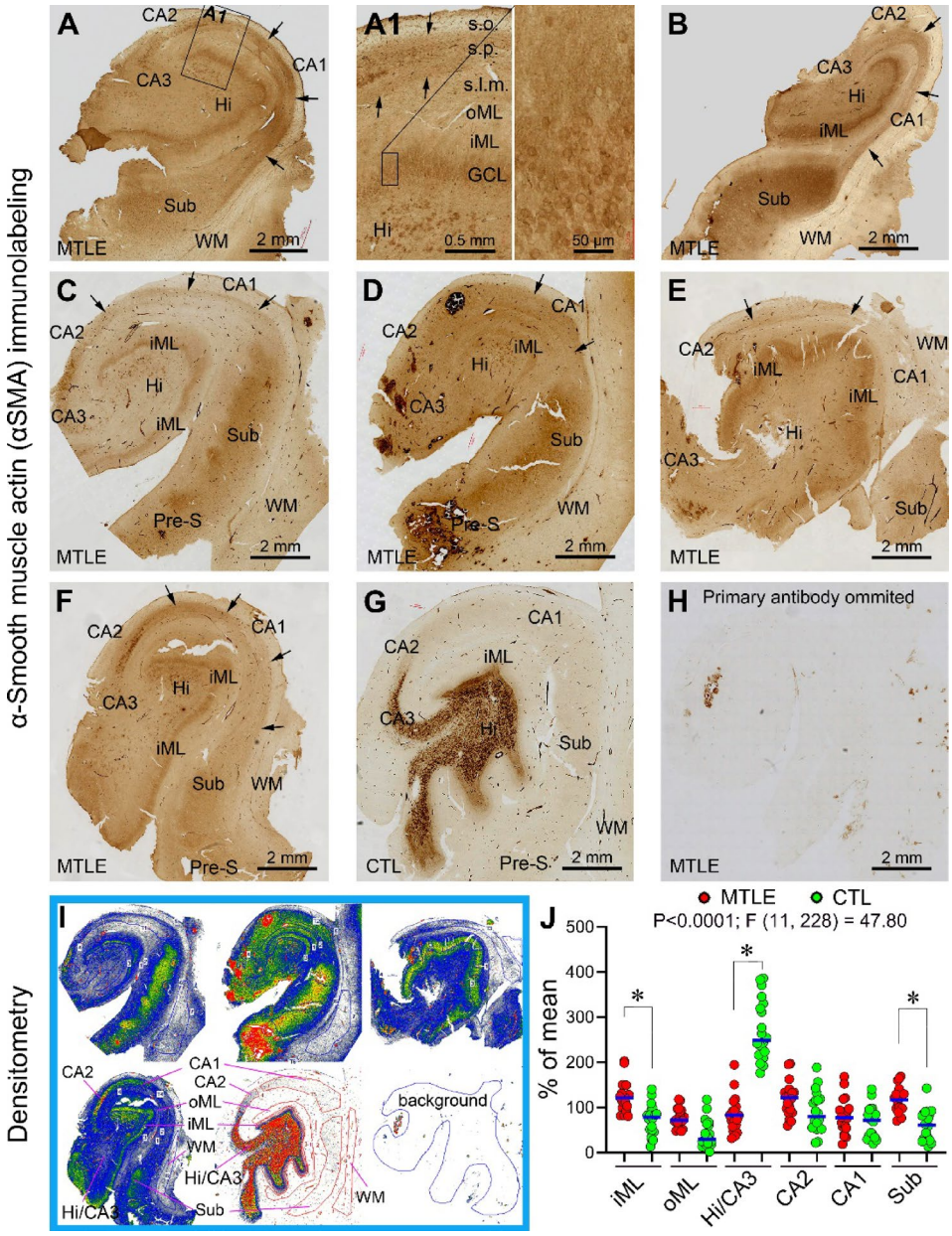

Fig. 3. Aberrant alpha-smooth muscle actin (αSMA) immunolabeling in resected hippocampi from patients with MTLE relative to postmortem control. Original micrographs show αSMA immunolabeled sections from 6 resected hippocampi (**A-F**), a postmortem control (**G**), and a parallelly processed section by excluding the primary antibody serving as assay control (**H**). αSMA immunolabeling appears to be reduced in the hilus (Hi) and CA3, increased in the inner molecular layer (iML) and the subicular subregions (Sub) in the resected relative to control sections. The dispersed granule cells are visible in mix with enhanced neuropil labeling in the iML (**A1**). The labeling pattern around CA2 and its joining CA3 and CA1 areas appears to be enhanced with some laminar disruption in the resected samples (**A**, **A1**, **C**, **F**), as compared to the typical wadge-shape ending of the MF terminals in the control hippocampus (**G**). The labeling in CA1 appears as a band (pointed by arrows) in the resected hippocampi (**A**, **B**, **C**, **D**, **E**, **F**), which is flattened in the samples with the CA1 area greatly shrunken (**B**, **E**). Panel **(I)** illustrates the densitometric method, with the areas of interest selected using the interconnecting drawing tool, avoiding blood clotting areas, torn/broken areas and large blood vessels. The optic density (o.d.) obtained from the white matter (WM) area is used as the cutoff for defining the specific o.d. in the areas of interest. The relative levels (% of mean) of αSMA labeling intensity is significantly (*) increased in the iML and Sub, reduced in the hilus/CA3 (**J**). Additional abbreviations: s.o.: stratum oriens; s.p.: stratum pyramidale; s.l.m.: stratum lacunosum-moleculare; Pre-S: presubiculum; WM: white matter. Scale bars are as indicated.

following Result as well as the Discussion sections. The most prominent changes were the loss of αSMA IR in the hilus and CA3 regions, resulting in a spot-like remaining IR within and outside the arc of the DG (Fig. 3A1). The iML was apparently widened with enhanced staining intensity, with the somata of granule cells also exhibited aSMA IR (Fig. 3A1, insert). The neuropil IR also appeared to be increased over the CA2, CA1 and subicular areas in the resected hippocampi relative to control (Fig. 3A-H), forming a band (pointed by arrows) extending from CA2, across the thinned CA1, and entering the subicular areas (Fig. 3A, A1, B-F). This band was much thinned and located deep to the stratum oriens (s.o.) in the heavily sclerotic hippocampi wherein the entire thickness of CA1 was dramatically narrowed (Fig. 3B, C, E).

Optic densitometry for αSMA IR was carried out in hippocampal subregions using the white matter area in the same section as a background cutoff (Fig. 3I). Areas were circled using the free-hand interconnecting tool by excluding cracked areas, large blood vessels, and areas occupied by blood clots (showed non-specific labeling as seen in batch-processed sections excluding the αSMA antibody incubation, Fig. 3H). Given that the intensity of αSMA IR is similar in the hilus and CA3[38] and it was difficult to define these subregions in the resected hippocampi, we measured the density over these areas together. Considering the influence of tissue fixation delay, we calculated the relative densities of the regions by normalizing the raw data to the overall means (based on all regions from all samples) of the two groups, respectively. The relative density levels (% of mean) of αSMA IR were 124.0 ± 33.7% (mean ± S.D., same below) vs. 72.3 ± 33.7% in the iML, and 76.3 ± 20.9% vs. 41.7 ± 29.8% in the oML, of the resected vs. control groups. The values were 84.8 ± 39.0% vs. 270.5 ± 66.2% in the hilus/CA3, 118.6 ± 37.3% vs. 89.3 ± 44.5% in the CA2, 80.8 ± 38.5% vs. 66.5 ± 35.1% in the CA1, and 115.5 ± 28.7% vs. 59.6 ± 33.8% in the Sub regions, in the resected hippocampi vs. control groups, respectively. Statistically, there was an overall difference among the regional means [$P < 0.0001$; F (DFn, DFd) = 47.8 (11, 228)], with the difference between the two groups reached statistical significance in the iML, hilus/CA3 and Sub by Tukey's multiple comparisons test (Fig. 3J).

Aberrant ZnT3 Immunolabeling in the resected hippocampi relative to control

ZnT3 is a well-established marker for normal and sprouting hippocampal MF terminals[7,47]. BACE1 is the enzyme initiating the amyloidogenic pathway of the β-amyloid precursor protein (APP) proteolysis, which is enriched at the MF terminals and can mark MF sprouting in pilocarpine-induced rodent model of temporal lobe epilepsy[11,48]. We used these two markers to cross-validate the MF sprouting pattern and to explore the extent thereof, if any, in the resected hippocampi, relative to that revealed by αSMA.

The labeling pattern and staining intensity of ZnT3 IR were significantly altered in the resected hippocampi relative to control (Fig. 4A-F). Thus, the iML was much widened with strong staining intensity in the surgical samples, while the oML also visualized. In the control samples, the IR delineated a narrow and distinct band along the iML, while the oML was barely visible. The IR was lost in the hilus and CA3 within the arc of the GCL among the resected hippocampi, with remaining labeling seen in other samples. In comparison, the IR filled the hilus and CA3 intensely and evenly in the postmortem control. The IR remained in CA2 and joining CA3 and CA2 areas CA1 as a band structure in the surgical samples, whereas the labeling in CA2 was weaker relative to the neighboring CA3 and CA1 areas in the control. The IR in CA1 and joining subicular subregions was greatly lost in some resected hippocampi, resulting in reduced intensity as low as that seen in the white matter (Fig. 4A, B, C). However, a thin band was visible near the s.o. even in these samples. In other resected hippocampi, ZnT3 IR in the CA1 area appeared as a fused band, but it separated into two bands along the borders of the s.p. and merged into the subicular areas wherein these bands were no longer recognizable (Fig. 4D, E, E1). These two bands appeared to be anatomically consistent with infra- and supra-pyramidal bundles of MF (IMF, SMF)[49], which could be highlighted because of the loss of axonal terminals in the region. In postmortem control, ZnT3 IR occurred across the CA1 and subicular subregions in an evenly distributed neuropil pattern (Fig. 4F).

Optic densitometry was carried out for ZnT3 IR using the same quantitative approach as described above for αSMA IR (Fig. 4G). There was an overall significant difference in the normalized data among the sample and regional groups [$P < 0.0001$; F (DFn, DFd) = 33.0 (11, 228)] (Fig. 4H). The relative values (% of mean) did not reach significant difference in the iML between the resected (132.0 ± 21.3%, mean ± S.D.) and control (125.6 ± 27.0%) groups, but reached significant difference in the oML (71.8 ± 23.3% vs. 41.2 ± 23.1%). The mean in CA2 was higher in the epilepsy (111.9 ± 20.1%) than control (81.7 ± 25.6%) groups. The mean was reduced with significant difference in the hilus/CA3 between the resected (79.4 ± 37.8%) vs. control (153.5 ± 21.9%) groups, as well as in the CA1 area (62.4 ± 33.7% vs. 120.4 ± 29.5%, same order). No statistical difference was reached for the values (122.7 ± 14.0% vs. 118.2 ± 27.0%) in the subicular areas (Fig. 4H).

Aberrant BACE1 Immunolabeling in the resected hippocampi relative to control

An altered pattern of BACE1 IR was also seen in the resected hippocampi relative to control. Thus, BACE1 IR appeared to be increased in the iML, while there was a loss of labeled MF terminals in the hilus and CA3 in the resected hippocampi (Fig. 5A-F). The remaining MF terminals in the hilus occurred in clusters along with lightly labeled mossy cells (Fig. 5E, E1). BACE1 IR appeared to be reduced in CA1 among most cases (Fig. 5A, C, D, E, F), but with a band remained deep to the s.o. in those with dramatic laminar thinning (Fig. 5C, E). The normalized levels (% of mean) of BACE1 IR was significantly increased in the iML (126.0 ± 25.7% vs. 88.4 ± 19.8%, resected vs. control, mean ± S.D., same format below) and in CA2 (116.0 ± 24.8% vs. 87.0 ± 23.2%), reduced in the hilus/CA3 (83.3 ± 34.5% vs. 153.6 ± 26.8%) as well as CA1 (74.8 ± 29.4% vs. 102.8 ± 25.9%) in the resected relative to control groups. No significant intergroup difference was reached for the values (117.2 ± 19.8% vs. 104.2 ± 25.0%) in the subicular subregions (Fig. 5G, H).

In the early phase of this study, we used sulphide fixation to prepare the resected hippocampi (a separate slice) along with fresh-froze postmortem human samples ($n = 4$/group) for concurrent Timm stain and immunohistochemical analysis (Fig. S1 A-J). However, the background was increased in the immunolabeled

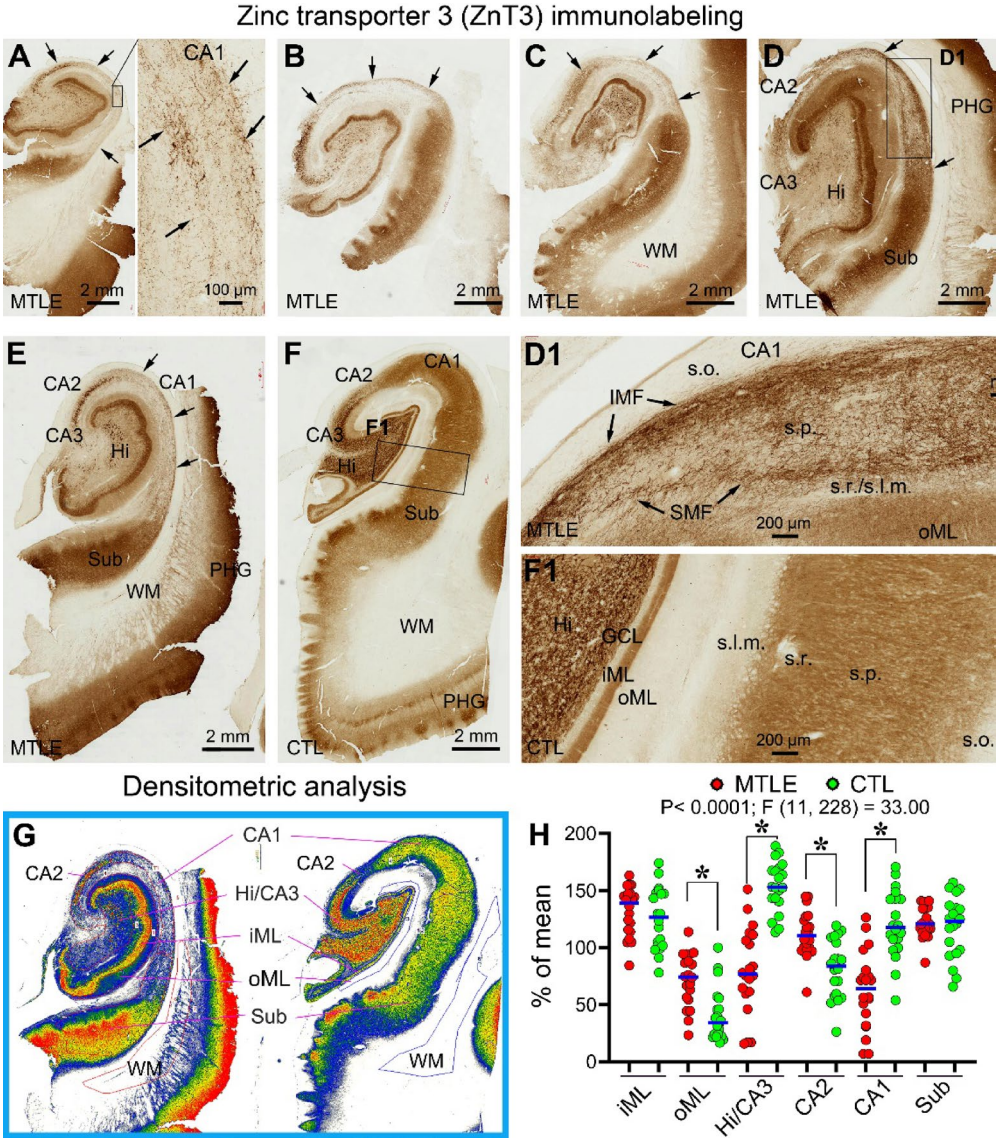

Fig. 4. Aberrant Zinc transporter 3 (ZnT3) immunolabeling in resected hippocampi from patients with MTLE relative to postmortem control. Micrographs show altered labeling in five resected samples (**A**, **B**, **C**, **D**, **E**, **D1**) relative to a control (**F**, **F1**). ZnT3 immunolabeling is dramatically lost in the hilus/CA3 and CA1 areas in the resected hippocampi. The inner molecular layer (iML) is apparently widened. The labeling intensity appears to be stronger in the iML, outer molecular layer (oML) and CA2 in the resected relative to control sections. The labeling in CA2 appears to extend into CA1 and remains as a band across CA1 and further entering the subicular regions. As moving from CA1 towards the Sub, this band is separated into fibrous bundles more densely located around the borders of the stratum pyramidale (s.o.), which appear to be consistent anatomically with the so-called infra- and supra-pyramidal mossy fiber bundles (IMF, SMF, pointed by arrows) (**A** and enlarged area, **D**, **D1**). The immunolabeling in the preserved subicular areas and temporal cortex (in a subset of samples) in the resected hippocampi appears neuropil-like (**A-E**), as is the labeling across CA1, Sub and the temporal cortex in the postmortem control (**F**, **F1**). The densitometric method and results are demonstrated in (**G**) and (**H**), with statistically significant intergroup difference marked by asterisks (*). Abbreviations are as defined in Fig. 3. Scale bars are as indicated.

sections with sulphide fixation compared to that seen in formalin fixation alone (Fig. S1 B, C, B1, C1, F, G, I, J). In addition, while the Timm stain could reveal the MF changes in the dentate gyrus in the resected hippocampi relative to control, it could not visualize the neuropil alterations seen in the CA and subicular regions as described above in αSMA, ZnT3 and BACE1 preparations (Fig. S2). Therefore, this histological approach was no longer used in the following experiments.

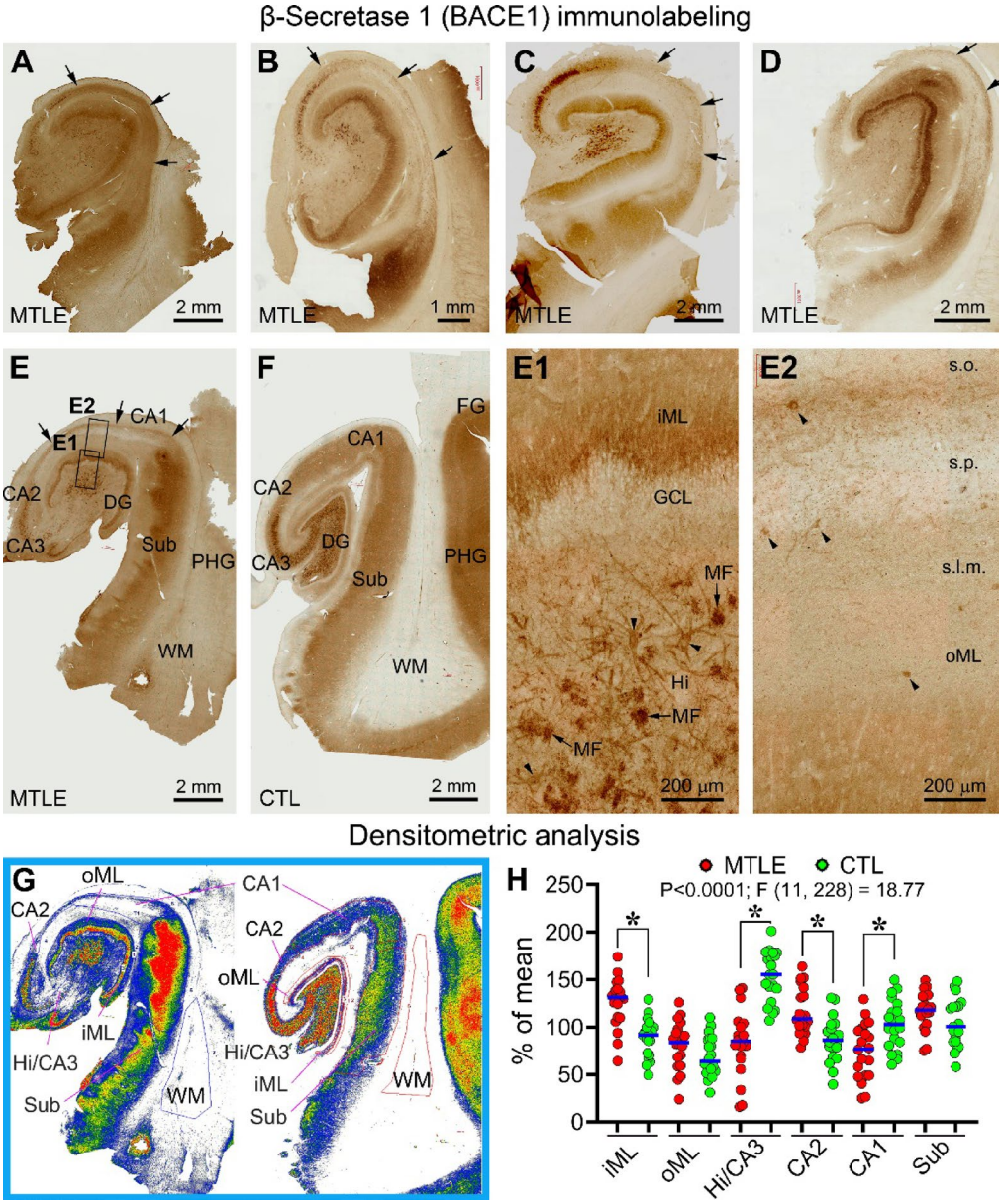

Fig. 5. Aberrant β-secretase 1 (BACE1) immunolabeling in resected hippocampi from patients with MTLE relative to postmortem control. Panels **(A-F)** show low magnification images, with the framed areas enlarged as indicated **(E1, E2)**. The mossy fiber (MF) labeling is reduced in the hilus and CA3, with the overall neuropil labeling in CA1 also reduced (with variability between cases) in the resected hippocampi **(A-E)** relative to control **(F)**. The labeling in the subiculum appears to be increased in some **(B, E)**, but reduced in other **(C, D)**, resected hippocampi. The labeling intensity in the iML and CA2 appears to be higher in the resected hippocampi than control. Also, a band-like labeling (arrows) remains in all resected hippocampi from CA2 across CA1 and extending into the subiculum. Mossy cells in the hilus and some remaining interneurons (arrowheads) in CA1 show light BACE1 labeling **(E1, E2)**. The remaining MF terminals in the hilus form chunk-like structures that are fairly large in size and distributed distantly in comparison with control **(E1**, arrows). **(G)** shows the methodology for measuring specific optic densities in hippocampal subregions using the white matter (WM) area as a background cutoff. **(H)** Graph and statistical results from one-way ANOVA analysis, with the * symbol indicating significantly intergroup difference. Scale bars are as indicated.

Aberrant COX Immunolabeling in the resected hippocampi relative to control

We explored potential regional alteration in mitochondrial oxidative metabolism in resected hippocampi relative to postmortem control using COX immunohistochemistry. Consistent with previously established histochemical staining pattern of this mitochondrial enzyme[50,51], COX IR exhibited a patchy distribution pattern (blobs) in layers III-IV in the primary visual cortex of postmortem human brains (Fig. 6A, A1). Also consistent with earlier findings[52,53], cortical interneurons exhibited heavy IR (Fig. 6A1 enlarged field).

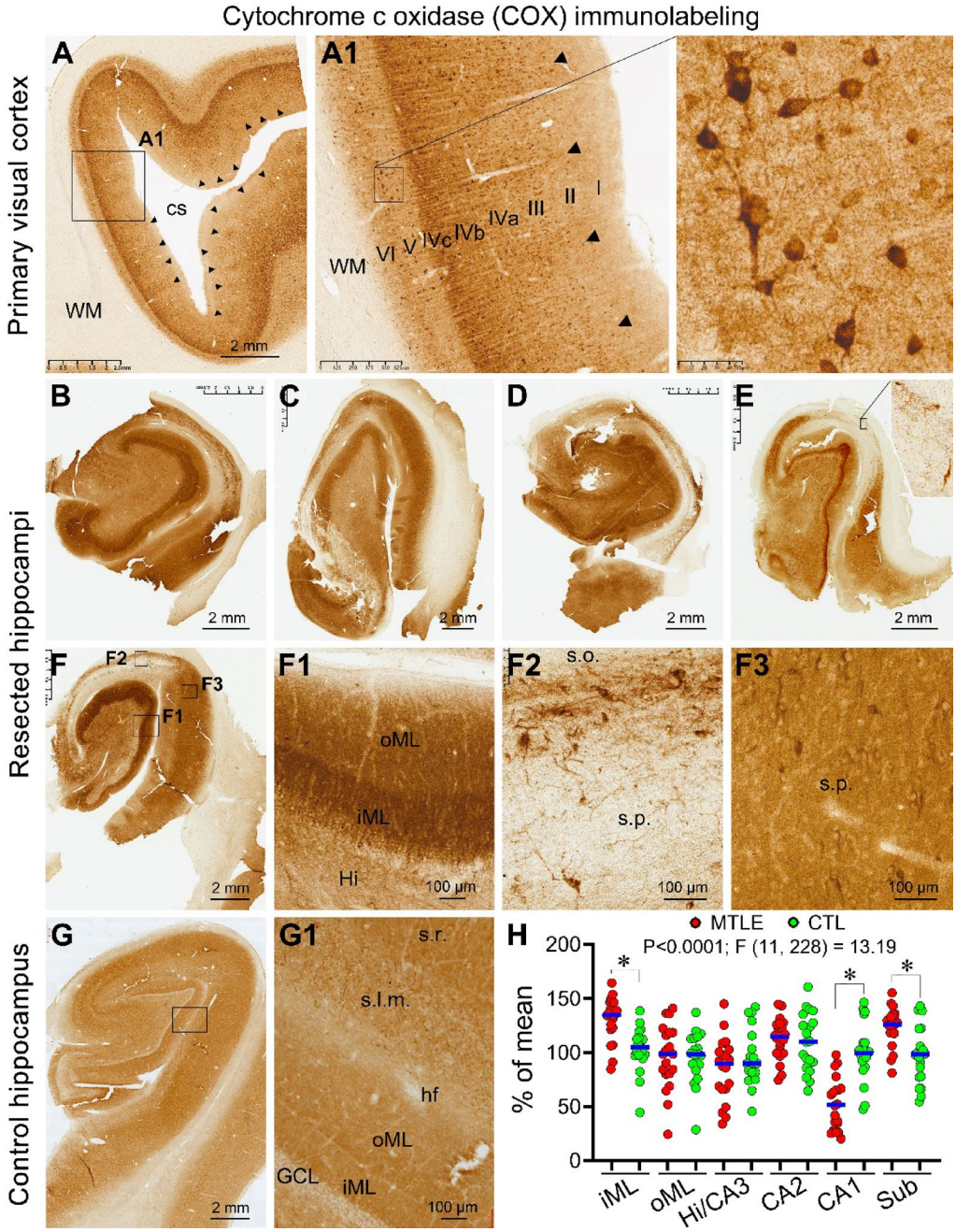

Fig. 6. Characterization of cytochrome c oxidase (COX) immunolabeling in the primary visual cortex and its alteration in resected hippocampi relative to postmortem control (CTL). Panels **(A, A1)** show COX immunolabeling in the primary visual cortex from an adult human brain. The characteristic patchy pattern in the supragranular layers is displayed, with the columnar blobs indicated by arrowheads. The labeled cells appear to be largely interneurons, with the most heavily labeled ones being likely the basket cells (**A1** and enlarged view). Panels (**B-F**) and enlarged fields (**F1**, **F2**, **F3**) show altered labeling in the resected hippocampi as compared with control (**G**, **G1**). The distribution and intensity of COX labeling vary significantly in the resected comparing to control hippocampal formation. The labeling appears to be reduced over the CA1 area except for a remaining band in the resected samples. The labeling intensity in the inner molecular layer (iML) and subiculum (Sub) appear to be higher in the resected sections, with a heavy labeling in CA2 in some cases (**D**, **E**). The labeling in all regions is predominantly neuropil-like in both the resected and control sections (**F1**, **F2**, **F3**, **G1**). However, in the resected hippocampi, a small number of somal profiles are labeled, with those in CA1 appearing to be interneurons (**F2**) and the ones in the subiculum appearing to be pyramidal neurons (**F3**). Quantitatively, the relative levels (% of mean) of COX labeling are significantly (*) decreased in CA1 and increased in the iML and subiculum in the resected group relative to control (**H**). Abbreviations: cs: calcarine sulcus; I-VI: cortical layers; WM: white matter; oML: outer molecular layer; s.o.: stratum oriens; s.p.: stratum pyramidale; s.l.m.: stratum lacunosum-moleculare; hf: hippocampal fissure. Scale bars are as indicated.

The regional and laminal distribution of COX IR was more differential in the resected hippocampi comparing with control (Fig. 6B-G). Thus, COX IR was heaviest in the iML and subicular areas in the resected hippocampi, which large involved an enhanced neuropil labeling by close examination (Fig. 6F, F1, F3). On the other hand, COR IR was reduced apparently in CA1, with some remained stained profiles that appeared to be interneurons and their dendritic processes (insert in Fig. 6E and F, F2). The normalized levels (% of mean) of COX IR showed an overall significant difference among the groups and regions [$P < 0.0001$, F (DFn, DFd) = 13.2 (11, 228)]. Thus, according to Tukey's multiple comparison posthoc tests, the values were significantly increased in the MTLE relative to control groups in the iML (130.9 ± 20.6% vs. 103.0 ± 20.2%) and Sub (123.5 ± 18.1% vs. 97.3 ± 26.1%), and reduced in CA1 (52.6 ± 23.9% vs. 100.1 ± 26.6%), while no intergroup differences were reached for the oML (96.1 ± 30.0% vs. 95.4 ± 23.4%), CA2 (112.7 ± 19.3% vs. 109.6 ± 26.8%) and the hilus/CA3 area (123.5 ± 18.1% vs. 97.3 ± 26.1%) (Fig. 6H).

Discussion

The hippocampus appears to be the major epileptogenic center in drug-resistant MTLE, as such surgical resection of this structure is used as a last solution to control seizure recurrence[54–56]. Aberrant interictal electrographic activities can be detected in the hippocampus in patients with MTLE[57], with dysfunctional communication existing between the hippocampus and extrahippocampal regions[58,59]. The cortical-hippocampal-cortical loop is a fundamental information processing system in the brain under normal conditions[60], which appears to be disrupted at least on two major relays of the trisynaptic circuitry, i.e., the hilus/CA3 and CA1, in MTLE as a result of neuronal death. The preserved dentate granule cells along with their reorganized MF connections are commonly considered to generate and output neuronal hyperactivity[9,61–64], while the subiculum may be also involved in the formation and propagation of epileptic activities[28,31,34,36,65]. The pathophysiology of MTLE remains puzzling in many aspects, with the anatomical/functional reorganization and interplay among the preserved neuronal populations, including those in the DG, CA2 and subiculum, potentially playing a critical role[17,66].

The resected hippocampi examined in the current study had significant neuronal loss. Thus, the numerical densities of NeuN-labeled neurons were reduced significantly in the hilus/CA3 and CA1, and also in CA2, although did not reach significant difference in the Sub, in the resected hippocampi relative to control. Similarly, the densities of sortilin-labeled neurons were significantly reduced in the resected samples in the hilus/CA3, CA1 and CA2, and also in Sub. The loss of sortilin-labeled cells also in the Sub might relate to the pyramidal neurons as this marker is primarily expressed in principal neurons[45,67–70].It should be noted that interneurons also die in sclerotic hippocampus in the hilus/CA3 and CA1, with the large-sized parvalbumin basket cells seemly most vulnerable.

MF sprouting into the iML is a consistent pathology in the hippocampus of MTLE patients and chronic epilepsy animal models as revealed in Timm stain and various immunolabeling preparations[11,39,47,71–76]. Studies have also shown that MF sprouting can extend into CA2[61,71,77]. In a recent study of 319 resected hippocampi from patients, synaptoporin-labeled axon terminals were observed in CA2, and even in CA1 in the specimens with relatively severe neuronal loss and granule cell dispersion[78]. Using retrovirus-based labeling technologies, MF sprouting into CA2 was observed in rats following pilocarpine-induced status epilepticus[79] and in mice following kainate-induced chronic seizures[80]. This pattern was also observed in epileptic transgenic mice expressing enhanced green fluorescent protein[78]. Long-range MF projection into the "regio superior" or CA1 exists naturally in some mammals such as hedgehog and cats, with aberrant sprouting occurring in this region in epileptic cats[49,81–83].

In the present study, αSMA, ZnT3 and BACE1 IR were reduced or dramatically lost in the hilus/CA3 in the resected hippocampi relative to control, consistent with a loss of MF and other axon terminals in these areas. The iML was widened with strong αSMA, ZnT3 and BACE1 IR in the resected hippocampi, indicating MF sprouting into this lamina. Consistent with the aforementioned findings of MF sprouting into CA2, the microscopic pattern and densitometric data showed a trend of, or statistically significant, increase of αSMA, ZnT3 and BACE1 IR in this region. The αSMA, ZnT3 and BACE1 IR over the CA1 and subicular areas exhibited some non-parallel alterations in the resected hippocampi. Specifically, a band-like αSMA IR was seen in CA1 with enhanced neuropil-like reactivity in the resected hippocampi, whereas the IR in control was background-like across regions except for a distinct labeling in the MF field. In comparison, BACE1 and ZnT3 IR were reduced in CA1 in the resected hippocampi, which should be related to axonal loss associated with neuronal loss in this region. However, a labeled band remained in CA1 and extended into the subicular areas. This band was flattened in the CA1 portion towards CA2 and separated into bundles as moving towards the subicular areas. In the latter, the tangentially running fibers were distributed more densely along the borders of the remaining pyramidal cell layer, which appeared to represent the so-called infrapyramidal and suprapyramidal MF bundles[49]. It should be noted that extents of change in a given anatomical area reflected by densitometry were not always matched between αSMA, ZnT3 and BACE1 IR. This discrepancy is conceivable because these markers are neither solely nor identically expressed in the MF. As such, confounding labeling (e.g., vascular, glial and non-MF axonal expression) would impact on the overall statistical outcomes.

Neuronal firing is ATP-dependent[84], as such neuronal overexcitability in epileptogenic hippocampus may rely on mitochondrial respiration. In this context, electron microscopic examination has found abundant presence of mitochondria in the reorganized MF terminals in the iML of human hippocampi[9]. Two previous studies (to the best of our knowledge) examined COX enzymatic activity with histochemistry in relatively small-sized ($n = 11$, in reference[85] ; and $n = 3$, in reference[86] resected hippocampi from patients with MTLE. Thus, COX activity was lost in the regions with cell loss, especially in CA1, while the enzyme activity was preserved[85] or unaffected[86] in the dentate molecular layer, CA2 and subiculum. Considering the impact of formalin fixation on histochemical enzyme reaction, immunohistochemistry was used in the present study. The laminar and cellular pattern of

COX IR in the primary visual cortex were confirmed to be consistent with established data[50–53]. With this cross-validation, we observed elevated COX IR in the iML and subiculum, and reduced IR in CA1. It should be noted that COX IR appeared not reduced in the hilus/CA3 in the resected hippocampi relative to control. This might relate to the presence of mitochondria in the reorganized MF terminals and/or gliosis in this region[19].

The current study has many limitations. First, the sample size was not large. The clinical data, including sex and age of the patients, age at seizure onset, frequency and duration of seizure, electroencephalographic and neuroimaging presentations, were fairly heterogenous. The sample size was not optimal for a stratified clinicopathological analysis. Second, for some reasons the aSMA labeling in the resected hippocampi exhibited high background noise. Given that the altered regional/laminar labeling pattern was detectable in the sections comparing to control, and that the surgical samples were "precious" and not conventionally available, we did not try various fixation/staining modifications to enhance the signal/background ratio (which could also cause issue of concern in comparative study). Thus, internal control approaches (threshold o.d. cutoff and data normalization) were used to assess the intergroup differences following identical processing procedures (staining, image acquisition and quantification). These approaches appeared to be fairly robust in regard to statistical analysis of group differences. For instance, the ZnT3 labeling in the inner molecular layer in the resected hippocampi appeared microscopically impressive, while its increase in intensity did not reach significant difference relative to control. Notably, ZnT3 labeling appeared also increased in the oML, with the relative values reached significant difference between the two groups, indicate that MF sprouting can reach the outer part of the molecular layer. Third, our interpretation of MF sprouting was based on pattern recognition along with densitometry. In this context, a few previous studies applied biocytin or neurobiotin to label the granule cells and their dendritic and axonal processes in resected human hippocampal slices in vitro[22,87,88]. This requires specialized laboratory settings and experimental skills. It is also uncertain whether these methods can trace long distance axonal pathway formed preoperationally in surgical human brain samples. A potential way to explore the existence of long-range MF sprouting, and the functional relevance to epileptogenesis thereof, if any, may be some preliminary microsurgical trials on drug-resistant MTLE patients. Anatomically, the fibrous band passes the CA1 area below and near the basal wall of the temporal lateral ventricle. It might be possible to ablate the passing fibers via intraventricular neuroendoscopy. Alternatively, precision-guided micro-lesion at the CA1 area such as by gamma-knife might also eliminate the passing fibers. Neuronal loss in the CA1 region would be already severe in the MTLE patients requiring neurosurgery, therefore, the effect of these microsurgical procedures on healthy neurons may be limited. Thus, close-cranial CA1 microsurgery may be worthy of consideration as an exploratory adventure of hippocampus-saving therapeutical intervention for drug-resistance MTLE.

Conclusion

MF sprouting beyond the iML and pathological changes in the preserved hippocampal regions have gained increasing attention in study of MTLE in humans and animal models. The present study characterized the alteration of αSMA, ZnT3, BACE1 and COX immunolabeling in the hippocampi from MTLE patients with disease characteristic neuronal loss. These markers visualized MF sprouting in the iML. αSMA labeling was present in the CA1 and Sub, with αSMA, ZnT3 and BACE1 labeling arranging as a fibrous band extending from CA2, CA1 to Sub in the epileptic samples. Heavy COX immunolabeling occurred in the iML and subiculum. These findings suggest the possibility of long-range MF sprouting and region-specific hypermetabolic capacity in the hippocampal formation of patients with drug resistant MTLE.

Data availability

All data needed to evaluate the conclusions in the paper are present in the paper and/or the Supplementary Materials. The raw data will be made available by the authors by contacting Tian Tu and Xiao-Xin Yan, without undue reservation.

Received: 9 June 2025; Accepted: 9 January 2026
Published online: 14 January 2026

References

1. Téllez-Zenteno, J. F. & Hernández-Ronquillo, L. A review of the epidemiology of temporal lobe epilepsy. *Epilepsy Res Treat.* 630853(2012). (2012).
2. Barba, C. et al. Temporal lobe epilepsy surgery in children and adults: A multicenter study. *Epilepsia* **62**, 128–142 (2021).
3. Thom, M. & Review Hippocampal sclerosis in epilepsy: A neuropathology review. *Neuropathol. Appl. Neurobiol.* **40**, 520–543 (2014).
4. Blümcke, I. et al. International consensus classification of hippocampal sclerosis in Temporal lobe epilepsy: A task force report from the ILAE commission on diagnostic methods. *Epilepsia* **54**, 1315–1329 (2013).
5. Amaral, D. G. & Dent, J. A. Development of the mossy fibers of the dentate gyrus: I. A light and electron microscopic study of the mossy fibers and their expansions. *J. Comp. Neurol.* **195**, 51–86 (1981).
6. Sloviter, R. S. A selective loss of hippocampal mossy fiber Timm stain accompanies granule cell seizure activity induced by perforant path stimulation. *Brain Res.* **330**, 150–153 (1985).
7. Wenzel, H. J., Cole, T. B., Born, D. E., Schwartzkroin, P. A. & Palmiter, R. D. Ultrastructural localization of zinc transporter-3 (ZnT-3) to synaptic vesicle membranes within mossy fiber boutons in the hippocampus of mouse and monkey. *Proc. Natl. Acad. Sci. U S A.* **94**, 12676–12681 (1997).
8. Pierce, J. P., Melton, J., Punsoni, M., McCloskey, D. P. & Scharfman, H. E. Mossy fibers are the primary source of afferent input to ectopic granule cells that are born after pilocarpine-induced seizures. *Exp. Neurol.* **196**, 316–331 (2005).
9. Zhang, N. & Houser, C. R. Ultrastructural localization of dynorphin in the dentate gyrus in human Temporal lobe epilepsy: A study of reorganized mossy fiber synapses. *J. Comp. Neurol.* **405**, 472–490 (1999).
10. Zhang, W., Thamattoor, A. K., LeRoy, C. & Buckmaster, P. S. Surviving mossy cells enlarge and receive more excitatory synaptic input in a mouse model of Temporal lobe epilepsy. *Hippocampus* **25**, 594–604 (2015).

11. Yan, X. X. et al. BACE1 elevation is associated with aberrant limbic axonal sprouting in epileptic CD1 mice. *Exp. Neurol.* **235**, 228–237 (2012).
12. Yan, X. X. et al. Chronic Temporal lobe epilepsy is associated with enhanced Alzheimer-like neuropathology in 3×Tg-AD mice. *PLoS One*. **7**, e48782 (2012).
13. Ribak, C. E. & Dashtipour, K. Neuroplasticity in the damaged dentate gyrus of the epileptic brain. *Prog Brain Res.* **136**, 319–328 (2002).
14. Dudek, F. E. & Sutula, T. P. Epileptogenesis in the dentate gyrus: A critical perspective. *Prog Brain Res.* **163**, 755–773 (2007).
15. Pallud, J. et al. Dentate gyrus and hilus transection blocks seizure propagation and granule cell dispersion in a mouse model for mesial Temporal lobe epilepsy. *Hippocampus* **21**, 334–343 (2011).
16. Nadler, J. V. The recurrent mossy fiber pathway of the epileptic brain. *Neurochem Res.* **28**, 1649–1658 (2003).
17. Houser, C. R. Hippocampal sclerosis in temporal lobe epilepsy: New views and challenges. *Jasper's Basic Mechanisms of the Epilepsies. 5th ed. New York: Oxford University Press*, 15–34 (2024).
18. Okazaki, M. M., Molnár, P. & Nadler, J. V. Recurrent mossy fiber pathway in rat dentate gyrus: synaptic currents evoked in presence and absence of seizure-induced growth. *J. Neurophysiol.* **81**, 1645–1660 (1999).
19. Gabriel, S. et al. Stimulus and potassium-induced epileptiform activity in the human dentate gyrus from patients with and without hippocampal sclerosis. *J. Neurosci.* **24**, 10416–10430 (2004).
20. Buckmaster, P. S. & Lew, F. H. Rapamycin suppresses mossy fiber sprouting but not seizure frequency in a mouse model of Temporal lobe epilepsy. *J. Neurosci.* **31**, 2337–2347 (2011).
21. Sloviter, R. S., Zappone, C. A., Harvey, B. D. & Frotscher, M. Kainic acid-induced recurrent mossy fiber innervation of dentate gyrus inhibitory interneurons: possible anatomical substrate of granule cell hyperinhibition in chronically epileptic rats. *J. Comp. Neurol.* **494**, 944–960 (2005).
22. Puhahn-Schmeiser, B., Leicht, K., Gessler, F. & Freiman, T. M. Aberrant hippocampal mossy fibers in Temporal lobe epilepsy target excitatory and inhibitory neurons. *Epilepsia* **62**, 2539–2550 (2021).
23. Spigelman, I. et al. Dentate granule cells form novel basal dendrites in a rat model of Temporal lobe epilepsy. *Neuroscience* **86**, 109–120 (1998).
24. Zhou, Q. G. et al. Chemogenetic Silencing of hippocampal neurons suppresses epileptic neural circuits. *J. Clin. Invest.* **129**, 310–323 (2019).
25. Sparks, F. T. et al. Hippocampal adult-born granule cells drive network activity in a mouse model of chronic Temporal lobe epilepsy. *Nat. Commun.* **11**, 6138 (2020).
26. Lybrand, Z. R. et al. A critical period of neuronal activity results in aberrant neurogenesis rewiring hippocampal circuitry in a mouse model of epilepsy. *Nat. Commun.* **12**, 1423 (2021).
27. Hendricks, W. D., Westbrook, G. L. & Schnell, E. Early detonation by sprouted mossy fibers enables aberrant dentate network activity. *Proc. Natl. Acad. Sci. U S A* 116, 10994–10999 (2019).
28. Cohen, I., Navarro, V., Clemenceau, S., Baulac, M. & Miles, R. On the origin of interictal activity in human Temporal lobe epilepsy in vitro. *Science* **298**, 1418–1421 (2002).
29. Staba, R. J., Wilson, C. L., Bragin, A., Fried, I. & Engel, J. Quantitative analysis of high-frequency oscillations (80–500 Hz) recorded in human epileptic hippocampus and entorhinal cortex. *J. Neurophysiol.* **88**, 1743–1752 (2002).
30. Vreugdenhil, M., Hoogland, G., Van Veelen, C. W. M. & Wadman, W. J. Persistent sodium current in subicular neurons isolated from patients with Temporal lobe epilepsy. *Eur. J. Neurosci.* **19**, 2769–2778 (2004).
31. Fabó, D. et al. Properties of in vivo interictal Spike generation in the human subiculum. *Brain* **131**, 485–499 (2008).
32. Wozny, C., Knopp, A., Lehmann, T. N., Heinemann, U. & Behr, J. The subiculum: A potential site of ictogenesis in human Temporal lobe epilepsy. *Epilepsia* **46**, 17–21 (2005).
33. Huberfeld, G. et al. Glutamatergic pre-ictal discharges emerge at the transition to seizure in human epilepsy. *Nat. Neurosci.* **14**, 627–634 (2011).
34. Kitaura, H. et al. Pathophysiological characteristics associated with epileptogenesis in human hippocampal sclerosis. *EBioMedicine* **29**, 38–46 (2018).
35. Xu, C. et al. Subicular pyramidal neurons gate drug resistance in Temporal lobe epilepsy. *Ann. Neurol.* **86**, 626–640 (2019).
36. Lévesque, M. & Avoli, M. The subiculum and its role in focal epileptic disorders. *Rev. Neurosci.* **32**, 249–273 (2020).
37. Fei, F., Wang, X., Wang, Y. & Chen, Z. Dissecting the role of subiculum in epilepsy: research update and translational potential. *Prog Neurobiol.* **201**, 102029 (2021).
38. Tu, T. et al. Mossy fiber expression of αSMA in human hippocampus and its relevance to brain evolution and neuronal development. *Sci. Rep.* **15**, 15834 (2025).
39. Blümcke, I. et al. Temporal lobe epilepsy associated up-regulation of metabotropic glutamate receptors: correlated changes in mGluR1 mRNA and protein expression in experimental animals and human patients. *J. Neuropathol. Exp. Neurol.* **59**, 1–10 (2000).
40. Yan, X. X., Ma, C., Bao, A. M. & Wang, X. M. Gai W. P. Brain banking as a cornerstone of neuroscience in China. *Lancet Neurol.* **14**, 136 (2015).
41. Qiu, W. et al. Standardized operational protocol for human brain banking in China. *Neurosci. Bull.* **35**, 270–276 (2019).
42. Amaral, D. G. & R I. Hippocampal formation. The Human Nervous System. *New York*: Academic 711–755 (1990).
43. Amaral, D. G., Fau, S. H. & Lavenex, P. The dentate gyrus: fundamental neuroanatomical organization (dentate gyrus for dummies). *Prog Brain Res.* **163**, 3–22 (2007).
44. Jiang, J. et al. Intraneuronal sortilin aggregation relative to granulovacuolar degeneration, Tau pathogenesis and Sorfra plaque formation in human hippocampal formation. *Front. Aging Neurosci.* **14**, 926904 (2022).
45. Xu, S. Y. et al. Regional and cellular mapping of sortilin immunoreactivity in adult human brain. *Front. Neuroanat.* **13**, 31 (2019).
46. Hu, X. et al. Sortilin fragments deposit at senile plaques in human cerebrum. *Front. Neuroanat.* **11**, 45 (2017).
47. Crèvecoeur, J. et al. Expression pattern of synaptic vesicle protein 2 (SV2) isoforms in patients with Temporal lobe epilepsy and hippocampal sclerosis. *Neuropathol. Appl. Neurobiol.* **40**, 191–204 (2014).
48. Zhang, S., Khanna, S. & Tang, F. R. Patterns of hippocampal neuronal loss and axon reorganization of the dentate gyrus in the mouse pilocarpine model of Temporal lobe epilepsy. *J. Neurosci. Res.* **87**, 1135–1149 (2009).
49. Gaarskjaer, F. The organization and development of the hippocampal mossy fiber system. *Brain Res.* **396**, 335–357 (1986).
50. Horton, J. C. & Hubel, D. H. Regular patchy distribution of cytochrome oxidase staining in primary visual cortex of macaque monkey. *Nature* **292**, 762–764 (1981).
51. Wong-Riley, M. T. T. et al. Cytochrome oxidase in the human visual cortex: distribution in the developing and the adult brain. *Vis. Neurosci.* **10**, 41–58 (1993).
52. Luo, X. G., Hevner, R. F. & Wong-Riley, M. T. T. Double labeling of cytochrome oxidase and γ-aminobutyric acid in central nervous system neurons of adult cats. *J. Neurosci. Methods.* **30**, 189–195 (1989).
53. Nie, F. & Wong-Riley, M. T. T. Double labeling of GABA and cytochrome oxidase in the macaque visual cortex: quantitative EM analysis. *J. Comp. Neurol.* **356**, 115–131 (1995).
54. Huberfeld, G., Blauwblomme, T. & Miles, R. Hippocampus and epilepsy: findings from human tissues. *Rev. Neurol. (Paris).* **171**, 236–251 (2015).
55. Shi, W. et al. Spike ripples localize the epileptogenic zone best: an international intracranial study. *Brain* **147**, 2496–2506 (2024).
56. Dong, H., Shi, J., Wei, P., Shan, Y. & Zhao, G. Comparative efficacy of surgical strategies for drug-resistant epilepsy: A systematic review and meta-analysis. *World Neurosurg.* **195**, 123729 (2025).

57. Pail, M. et al. High frequency oscillations in epileptic and non-epileptic human hippocampus during a cognitive task. *Sci. Rep.* **10**, 18147 (2020).
58. Mendes, R. A. V. et al. Hijacking of hippocampal-cortical oscillatory coupling during sleep in Temporal lobe epilepsy. *Epilepsy Behav.* **121**, 106608 (2021).
59. Hu, J. et al. Interictal suppression in patients with mesial Temporal lobe epilepsy: A simultaneous PET/fMRI study. *Neuroimage* **314**, 121207 (2025).
60. Rothschild, G., Eban, E. & Frank, L. M. A cortical–hippocampal–cortical loop of information processing during memory consolidation. *Nat. Neurosci.* **20**, 251–259 (2017).
61. Wittner, L. et al. The epileptic human hippocampal Cornu ammonis 2 region generates spontaneous interictal-like activity in vitro. *Brain* **132**, 3032–3046 (2009).
62. Krook-Magnuson, E. et al. In vivo evaluation of the dentate gate theory in epilepsy. *J. Physiol.* **593**, 2379–2388 (2015).
63. Dengler, C. G., Yue, C. & Takano, H. Coulter D. A. Massively augmented hippocampal dentate granule cell activation accompanies epilepsy development. *Sci. Rep.* **7**, 42090 (2017).
64. Kahn, J. B., Port, R. G., Yue, C. & Takano, H. Coulter D. A. Circuit-based interventions in the dentate gyrus rescue epilepsy-associated cognitive dysfunction. *Brain* **142**, 2705–2721 (2019).
65. de Guzman, P. et al. Subiculum network excitability is increased in a rodent model of Temporal lobe epilepsy. *Hippocampus* **16**, 843–860 (2006).
66. Whitebirch, A. C. et al. Enhanced excitability of the hippocampal CA2 region and its contribution to seizure activity in a mouse model of Temporal lobe epilepsy. *Neuron* **110**, 3121–3138e8 (2022).
67. de Lanerolle, N. C., Kim, J. H., Robbins, R. J. & Spencer, D. D. Hippocampal interneuron loss and plasticity in human Temporal lobe epilepsy. *Brain Res.* **495**, 387–395 (1989).
68. Mathern, G. W., Babb, T. L., Vickrey, B. G., Melendez, M. & Pretorius, J. K. The clinical-pathogenic mechanisms of hippocampal neuron loss and surgical outcomes in Temporal lobe epilepsy. *Brain* **118**, 105–118 (1995).
69. Sperk, G., Hamilton, T. & Colmers, W. F. Neuropeptide Y in the dentate gyrus. *Prog Brain Res.* **163**, 285–297 (2007).
70. Toth, K. & Magloczky, Z. The vulnerability of calretinin-containing hippocampal interneurons to Temporal lobe epilepsy. *Front. Neuroanat.* **8**, 100 (2014).
71. Houser, C. R. et al. Altered patterns of dynorphin immunoreactivity suggest mossy fiber reorganization in human hippocampal epilepsy. *J. Neurosci.* **10**, 267–282 (1990).
72. Proper, E. A. et al. Immunohistochemical characterization of mossy fibre sprouting in the hippocampus of patients with pharmaco-resistant Temporal lobe epilepsy. *Brain* **123**, 19–30 (2000).
73. Furtinger, S. et al. Plasticity of Y1 and Y2 receptors and neuropeptide Y fibers in patients with Temporal lobe epilepsy. *J. Neurosci.* **21**, 5804–5812 (2001).
74. Van Der Hel, W. S. et al. Hippocampal distribution of vesicular glutamate transporter 1 in patients with Temporal lobe epilepsy. *Epilepsia* **50**, 1717–1728 (2009).
75. Schmeiser, B., Zentner, J., Prinz, M., Brandt, A. & Freiman, T. M. Extent of mossy fiber sprouting in patients with mesiotemporal lobe epilepsy correlates with neuronal cell loss and granule cell dispersion. *Epilepsy Res.* **129**, 51–58 (2017).
76. Prada Jardim, A. et al. Characterising subtypes of hippocampal sclerosis and reorganization: correlation with pre and postoperative memory deficit. *Brain Pathol.* **28**, 143–154 (2018).
77. Cook, T. M. & Crutcher, K. A. Lesion-induced CA1 mossy fibers in the rat represent a neoinnervation. *Exp. Brain Res.* **70**, 433–436 (1988).
78. Freiman, T. M. et al. Mossy fiber sprouting into the hippocampal region CA2 in patients with Temporal lobe epilepsy. *Hippocampus* **31**, 580–592 (2021).
79. Althaus, A. L., Zhang, H. & Parent, J. M. Axonal plasticity of age-defined dentate granule cells in a rat model of mesial Temporal lobe epilepsy. *Neurobiol. Dis.* **86**, 187–196 (2016).
80. Häussler, U., Rinas, K., Kilias, A., Egert, U. & Haas, C. A. Mossy fiber sprouting and pyramidal cell dispersion in the hippocampal CA2 region in a mouse model of Temporal lobe epilepsy. *Hippocampus* **26**, 577–588 (2016).
81. Gaarskjaer, F. B., Danscher, G. & West, M. J. Hippocampal mossy fibers in the Regio superior of the European Hedgehog. *Brain Res.* **237**, 79–90 (1982).
82. Laurberg, S. & Zimmer, J. Aberrant hippocampal mossy fibers in cats. *Brain Res.* **188**, 555–559 (1980).
83. Blaabjerg, M. & Zimmer, J. The dentate mossy fibers: structural organization, development and plasticity. *Prog Brain Res.* **163**, 85–107 (2007).
84. Li, S. & Sheng, Z. H. Energy matters: presynaptic metabolism and the maintenance of synaptic transmission. *Nat. Rev. Neurosci.* **23**, 4–22 (2021).
85. Brines, M. L. et al. Regional distributions of hippocampal Na+, k(+)-ATPase, cytochrome oxidase, and total protein in Temporal lobe epilepsy. *Epilepsia* **36**, 371–383 (1995).
86. Opačić, M. et al. Regional distribution of cytochrome c oxidase activity and copper in sclerotic hippocampi of epilepsy patients. *Brain Behav.* **11**, e01986 (2020).
87. Isokawa, M., Levesque, M. F., Babb, T. L. & Engel, J. Jr. Single mossy fiber axonal systems of human dentate granule cells studied in hippocampal slices from patients with Temporal lobe epilepsy. *J. Neurosci.* **13**, 1511–1522 (1993).
88. Lim, C., Blume, H. W., Madsen, J. R. & Saper, C. B. Connections of the hippocampal formation in humans: I. The mossy fiber pathway. *J. Comp. Neurol.* **385**, 325–351 (1997).

Acknowledgements

We thank Jian Jiang, Jia-Qi Ai, Yan Wang, Xiao-Lu Cai and Sidiki Coulibaly for human brain banking and histo-pathological evaluation, and Xiao-Hua Tan, Ming-Li Zhang for help with light microscopic imaging.

Author contributions

All authors read and approved the final version of the manuscript. Conceptualization and study design: XXY, ZYL; Methodology: TT, LW, CY, HSZ; Data acquisition and analysis: QLZ, ZPS, TT; Writing - original draft preparation: TT, XXY; Writing - review and editing: XXY; Funding acquisition: XXY, TT, AP, ET, ZYL; Resources: HYL, BST, ET, JW, ZQW, ZYL.

Funding

This study was supported by National Natural Science Foundation of China (#82071223 to XXY; #82201595 to TT), Ministry of Science and Technology of China (grant #2021ZD0201103 and 2021ZD02018 to XXY, AP), and Hunan Provincial Science & Technology Foundation (#2020SK2122 to ET, and #2023JJ30908 to ZYL).

Declarations

Competing interests
The authors declare no competing interests.

Ethics approval
The surgical procedure and pathological examination of resected brain tissues were carried out with written consent from the patients and family members. All human brains were banked with written informed consent obtained prior to post-mortem donation from the donor and/or the next-of kin. The Ethics Committee for Research and Education at Xiangya School of Medicine approved the use of postmortem human materials.

Additional information
Supplementary Information The online version contains supplementary material available at https://doi.org/10.1038/s41598-026-36148-3.

Correspondence and requests for materials should be addressed to T.T., Z.-Y.L. or X.-X.Y.

Reprints and permissions information is available at www.nature.com/reprints.

Publisher's note Springer Nature remains neutral with regard to jurisdictional claims in published maps and institutional affiliations.